IEEE Access
Multidisciplinary ⋮ Rapid Review ⋮ Open Access Journal

Received July 3, 2020, accepted July 12, 2020, date of publication July 16, 2020, date of current version July 28, 2020.

Digital Object Identifier 10.1109/ACCESS.2020.3009694

Multi-Physical Coupling Field Study of 500 kV GIL: Simulation, Characteristics, and Analysis

HAIQING NIU[1], (Member, IEEE), ZEMING CHEN[1], HUANG ZHANG[1], XIN LUO[2], XIAOLIANG ZHUANG[2], XIAOXIAO LI[1], AND BO YANG[3]

[1]School of Electric Power, South China University of Technology, Guangzhou 510640, China
[2]EHV Power Transmission Company, China Southern Power Grid, Guangzhou 510640, China
[3]Faculty of Electric Power Engineering, Kunming University of Science and Technology, Kunming 650500, China

Corresponding author: Zeming Chen (1172454133@qq.com)

This work was supported in part by Guangzhou Bureau, China Southern Grid Extra High Voltage (CSG EHV) Power Transmission Company.

ABSTRACT With the construction of a large number of hydropower stations, transmission lines crossing a river and urban utility tunnels, gas insulated transmission line (GIL) has been applied widely due to its large transmission capacity, low environmental impact and high reliability. Accurate modelling of physical quantities and their characteristics of GIL provides a theoretical basis for its design and operation, which is of great significance to ensure the safety and reliability of GIL operation. The mathematical model and their relationship of GIL multi-physical fields are analyzed at first, upon which simulation model of GIL is built. Secondly, multi-physical coupling field model of electric, magnetic, thermal, fluid and stress field for GIL is studied, while simulation results are basically in consistent with experimental data to verify effectiveness of the model. Thirdly, distribution of multi-physical fields and their relationship are simulated and analyzed, while proximity effect, edge effect and compression factor of GIL multi-physical field are discussed. The results show that the radial temperature inside GIL is higher at the top, lower at the bottom, leading to uneven distribution of thermal expansion displacement, while the axial temperature distribution is basically uniform, which falls firstly and then rises near basin insulator thus results in edge effect. Proximity effect leads to asymmetric distribution and a slight increase of temperature inside GIL as well as a dramatic increase of air velocity around GIL. In addition, when ambient temperature is lower than −5 °C, the compression factor is much lower than 1 and the effect of compression factor should be considered in simulation.

INDEX TERMS GIL, multi-physical coupling field, finite element method, multi-physical characteristics.

I. INTRODUCTION

Gas Insulated Transmission Line (GIL) is a high-voltage power transmission equipment, insulated by SF_6 gas or SF_6 mixture or compressed air, with enclosures and conductors arranged coaxially [1]. GIL has the advantages of large transmission capacity, less power loss, low environmental impact, long service life, and high reliability [2], [3]. In recent years, it has been widely used in hydropower stations, power transmission projects across river basins, under-ground tunnels and other projects [4].

With the development of computational high-voltage engineering, visualization and precise quantification of physical process can be realized by calculating and simulating multi-physical coupling fields [5]. At present, research on multi-physical coupling field of electrical equipment has become one of the hottest topics. The overall length of GIL increases annually which is accompanied with the increase of defects during operation, such as abnormal sound, gas leakage and insulators crack. Therefore, establishing a multi-physical coupling field simulation model of GIL and studying characteristics of each physical field is of great significance to ensure its operation safety and reliability, which can provide a theoretical basis for design and optimization of its structure, as well as solve practical engineering problems.

During GIL operation, conductor current induces eddy current. Current losses on conductor and enclosures cause their temperature rise, resulting in thermal expansion and gas flow inevitably. The above process involves simultaneous interactions between electric, magnetic, thermal, fluid and stress fields, so it is necessary to study the characteristics of each physical field and their mutual influence. Many researches about magnetic-thermal-fluid coupling simulation and thermal-stress field coupling simulation have been carried out.

The associate editor coordinating the review of this manuscript and approving it for publication was Fabio Massaro.

In terms of coupling calculation of magnetic-thermal-fluid model, Qiao *et al.* [6] used finite element method and multi-physics coupling, heat transfer properties were analyzed by a three-dimensional axisymmetric GIL model under different gas pressures, conductor currents and ambient temperatures. Doukas *et al.* [7] presented a coupled electro-thermal model for transient analysis of GIL. The finite-difference time-domain method was adopted to calculate electrical parameters, heat transfer equations were derived and temperature distribution over space and time was calculated based on volume-element-method. Besides, Wang *et al.* [8] used ANSYS APDL-Cfx coupling methods to establish a model for medium voltage switchgear, and carried out simulation and analysis based on electromagnetic-thermal-fluid field. Dhotre *et al.* [9] developed electromagnetic fluid temperature simulation model for high-voltage circuit breaker, and analyzed its temperature rising characteristics, while symmetrical boundary conditions are proposed to simplify the model and to reduce the calculation burden. Additionally, Wu *et al.* [10] built an electromagnetic-fluid-thermal coupling simulation model for three-phase gas insulated bus and analyzed temperature distribution and characteristics, considering temperature characteristics of SF_6 gas based on Sutherland's law.

On the other hand, in the aspect of coupling calculation involving stress field, Zhong [11] calculated three-dimensional finite element models of electric field, electrodynamic field and thermal-fluid field. Wang *et al.* [12] established a GIL thermal-flow-stress coupling model to calculate stress field distribution, together with a correlation analysis of axial thermal strain.

The main differences of this work in comparison with previous researches can be summarized as the following three aspects:

- A multi-physical model of GIL is built in this paper, and the relations between electric, magnetic, thermal, fluid and stress filed are fully considered and coupled, which is more comprehensive and accurate. Particularly, magnetic-thermal-fluid field is directly coupled and thermal-stress is sequentially coupled. In contrast, work [6]–[10] only considered current loss as heat source for thermal field without considering thermal influence on metal conductivity, which means the magnetic-thermal field is sequentially coupled rather than directly coupled.
- The proximity effect and edge effect of thermal-fluid field are analysed in this paper. In contrast, work [13], [14] analysed the electromagnetic proximity effect of cable bundle and voltage transformer respectively. Since metal enclosure of GIL is grounded, there is no electromagnetic proximity effect between adjacent GIL, the analysis of proximity effect in this paper focuses on thermal-fluid field under GIL multi-phase parallel operation, which is a further consideration for GIL actual operation. In addition, compared with work [15], which only considered electric edge effect of capacitors, this work focused on GIL edge effect of thermal field resulted from basin insulators and length of GIL element on axial temperature distribution.
- The influence of compression factor on thermal-fluid field is considered and analysed. In contrast, work [16] only calculated SF6 gas compression factor under different pressures and temperature. Moreover, this work introduces compression factor to thermal-fluid equations through iteration, which considers GIL temperature deviation caused by gas density deviation.

In this paper, a three-dimensional electric-magnetic-thermal-fluid-stress coupling model for GIL is established to simulate its actual operation by finite element method. Simulation results are compared with temperature rise experiment and thermal strain experiment to verify model effectiveness. Distribution of each physical field is analyzed and studied. The proximity effect, edge effect and compression factor of multi-physical fields are discussed.

II. MATHEMATICAL MODELLING

A. BASIC PHYSICAL FIELD

During GIL operation, heat is generated when current flows through its conductor which results in the temperature rise in simulation domain, then gas flow and thermal expansion of conductor and enclosure. Therefore, this paper deals with the coupling relationship between electricity, magnetism, heat, fluid and stress.

Poisson's equation can be used to describe potential distribution under a certain voltage, as follows

$$\begin{cases} \nabla^2\phi = -\frac{\rho_s}{\varepsilon} \\ \boldsymbol{E} = -\nabla\phi \end{cases} \tag{1}$$

where ∇^2 is the Laplace operator, ϕ is the electric potential, ρ_s is the charge density, ε is the dielectric constant, and $\boldsymbol{E}$ is the electric intensity, respectively.

Equation about eddy current can be used to describe magnetic vector potential distribution under a certain current by

$$\begin{cases} \nabla(\nabla\cdot\boldsymbol{A}) - \nabla^2\boldsymbol{A} = \mu\boldsymbol{J_s} \\ \boldsymbol{B} = \nabla\times\boldsymbol{A} \end{cases} \tag{2}$$

where $\boldsymbol{A}$ is the magnetic vector potential, μ is the permeability, $\boldsymbol{J_s}$ is the source current density vector, and $\boldsymbol{B}$ is the magnetic flux density, respectively.

Heat conduction, convection and radiation can be described as

$$\rho c\frac{\partial T}{\partial t} = \nabla\cdot(\lambda\nabla T) + \boldsymbol{\Phi} \tag{3}$$

$$q = h\Delta T \tag{4}$$

$$\boldsymbol{\Phi} = \varepsilon_1 A_1\sigma(T_1^4 - T_2^4) \tag{5}$$

where ρ is the material density, c is the specific heat capacity, λ is the thermal conductivity, $\boldsymbol{\Phi}$ is the energy generated per unit volume per unit time, T is the temperature, t is the time, ΔT is the temperature difference between the fluid and the object surface, h is the convective heat transfer coefficient,

q is the heat flux, A_1 is the surface area, T_1 is the surface temperature of the surrounded object, ε_1 is the surface emissivity, T_2 is the surface temperature of the cavity object, and σ is the Stefan Boltzmann constant, respectively.

Consider mass conservation, momentum conservation and energy conservation, equations about fluid field can be written as

$$\frac{\partial \rho}{\partial t} + \nabla(\rho \cdot \boldsymbol{v}) = 0 \tag{6}$$

$$\rho \frac{\partial \boldsymbol{v}}{\partial t} + \rho(\boldsymbol{v} \cdot \nabla)\boldsymbol{v} = \nabla \cdot [-P + \eta(\nabla \boldsymbol{v} + (\nabla \boldsymbol{v})^T)] + \boldsymbol{F} \tag{7}$$

$$\frac{\partial T}{\partial t} + \boldsymbol{v} \cdot \nabla T = \frac{\lambda}{\rho c_p} \nabla^2 T \tag{8}$$

where c_p is the specific heat capacity at constant pressure, P is the pressure, η is the dynamic viscosity, $\boldsymbol{v}$ is the fluid velocity vector, and $\boldsymbol{F}$ is the volume force vector, respectively.

In stress field, due to the effect of thermal stress, the conductor and enclosure will produce thermal strain, which yields

$$\frac{\partial \boldsymbol{\sigma}}{\partial x} + \boldsymbol{F} = \rho \frac{\partial^2 \boldsymbol{u}}{\partial t^2} + \mu \frac{\partial \boldsymbol{u}}{\partial t} \tag{9}$$

$$\begin{cases} \varepsilon_{ij} = \dfrac{1}{2}\left(\dfrac{\partial u_i}{\partial x_j} + \dfrac{\partial u_j}{\partial x_i}\right) \\ \varepsilon_{ij} = \varepsilon_{ij}^{E} + \varepsilon_{ij}^{Th} \end{cases} \tag{10}$$

where $\boldsymbol{F}$ is the external force, σ is the stress tensor, u is the displacement, $\boldsymbol{u}$ is the damping coefficient, ε_{ij} is the strain tensor, $\varepsilon_{ij}^{\mathrm{E}}$ is the elastic strain component, and $\varepsilon_{ij}^{\mathrm{Th}}$ is the thermal strain component, respectively.

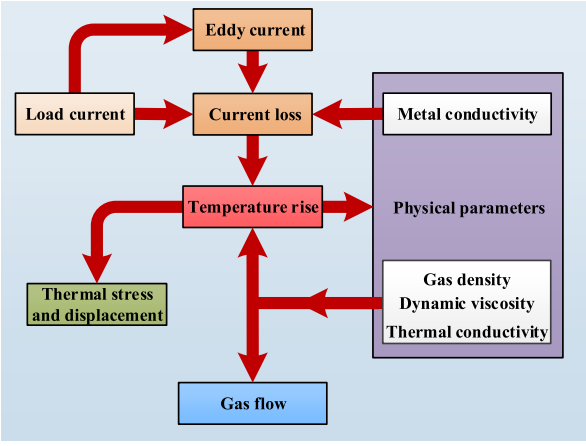

FIGURE 1. Coupling relationship between GIL multi-physical fields.

B. COUPLING RELATIONSHIP OF MULTI-PHYSICAL FIELDS

1) INTERACTION OF PHYSICAL QUANTITIES

When GIL is in normal operation, physical fields interact and correlate with each other, which relationship is shown in Fig. 1. Generally, GIL operates in an alternating electric field, which will produce displacement current and affect its magnetic field. However, due to low frequency and tiny displacement current of GIL, the interaction of electric field and magnetic field is insignificant and can be ignored. Therefore, influence between electric field and magnetic field is not considered in this paper.

Current loss in conductor and enclosure is heat source for thermal field. A change of temperature will affect metal conductivity and then current loss, while it will change gas density, dynamic viscosity and thermal conductivity and then affect gas velocity. Meanwhile, gas flow will carry heat away and change its temperature distribution. Therefore, the dependent variables among magnetic field, thermal field and fluid field are directly correlated.

On the other hand, temperature rise causes thermal stress and expansion displacement, while comparing with GIL element length, the displacement is small enough to influence other fields, so thermal field and stress field are sequentially coupled.

2) RELATIONSHIP OF MAGNETIC-THERMAL-FLUID FIELD

Conductivity of GIL conductor and enclosure is affected by temperature. Therefore, coupling relationship between magnetic field and thermal field can be described by Eq. (11) and Eq. (12), respectively.

$$Q_v = \boldsymbol{J} \cdot \boldsymbol{E} = \frac{1}{\boldsymbol{\sigma}} |\boldsymbol{J}|^2 \tag{11}$$

$$\sigma = \frac{\sigma_{ref}}{1 + \alpha\,(T - T_{\mathrm{ref}})} \tag{12}$$

where Q_{v} is the current loss per unit volume, α is the temperature coefficient of conductivity, σ_{ref} is the metal conductivity at reference temperature T_{ref}, which is 20 °C, respectively.

Consider direct coupling relationship between thermal field and fluid field, temperature change leads to a change of gas density and pressure, which affects flow velocity, while flow velocity of fluid affects its temperature distribution. Therefore, Eq. (3) and Eq. (8) can be combined to describe coupling relationship between thermal field and fluid field, as follows

$$\begin{cases} \rho(T) c_{\mathrm{p}} \dfrac{\partial T}{\partial t} + \rho(T) c_{\mathrm{p}} \boldsymbol{v} \cdot \nabla T = \nabla \cdot (\lambda \nabla T) + \boldsymbol{\Phi} \\ \rho(T) = \dfrac{PM}{RT} \end{cases} \tag{13}$$

where P is the gas pressure, M is the gas molar mass, T is the gas temperature, R is the ideal gas constant, respectively.

Hence, coupling relationship among magnetic field, thermal field and fluid field can be described by Eq. (14).

$$\rho(T) c_{\mathrm{p}} \frac{\partial T}{\partial t} + \rho(T) c_{\mathrm{p}} \boldsymbol{v} \cdot \nabla T = \nabla \cdot (\lambda \nabla T) + \frac{1}{\boldsymbol{\sigma}} |\boldsymbol{J}|^2 \tag{14}$$

3) RELATIONSHIP OF THERMAL-STRESS FIELD

In stress field, thermal expansion displacement is caused by thermal rise, but not affect other physical fields due to the displacement small enough comparing with GIL size. The coupling relationship between thermal field and stress field can be described by [17]

$$\varepsilon^{\mathrm{Th}} = \alpha_{\mathrm{p}} \Delta T = \alpha_{\mathrm{p}} (T - T_{\mathrm{am}}) \tag{15}$$

where α_p is the coefficient of linear thermal expansion and T_{am} is the ambient temperature.

Combine Eq. (15) and Eq. (10), displacement distribution and stress distribution can be calculated accordingly.

III. GEOMETRIC MODEL OF 500 kV GIL

The basic structure of 500 kV GIL is illustrated in Fig. 2, which mainly includes metal enclosure, inner conductor, post insulator, basin insulator and particle trap.

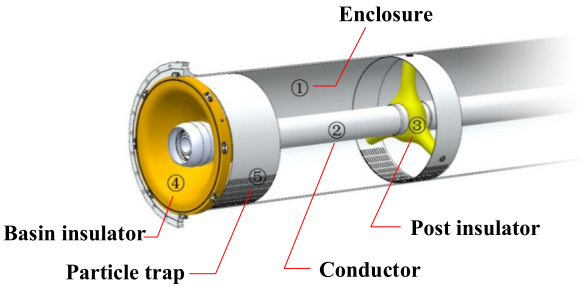

FIGURE 2. Basic structure of GIL.

Reference [12] and [18] separately carried out temperature rise experiment and thermal strain experiment of single-phase GIL element. Based on the experiments, this paper studies correctness of multi-physical field simulation model in section IV D and F.

The phase voltage of GIL is 289 kV and the current is 5600 A. The boundary condition of simulation is consistent with experimental environment. The multi-physical field of GIL is calculated by COMSOL Multiphysics.

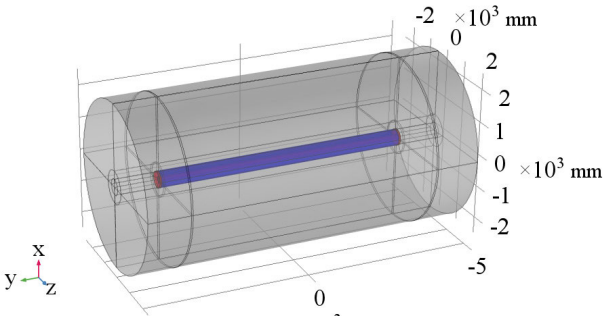

FIGURE 3. Finite element model of 500 kV GIL.

The geometric model of the simulation is demonstrated in Fig. 3, in which GIL element length is 7.5 m and simulation domain is a cylinder with 5000 mm diameter and 10000 mm length.

The parameters of conductor and enclosure are presented in Table 1, while gas parameters of air and SF_6 gas are tabulated in Table 2.

IV. SIMULATION STUDIES AND MODEL VERIFICATION

A. TEMPERATURE RISE EXPERIMENT AND THERMAL STRAIN EXPERIMENT

In temperature rise experiment, GIL element was placed horizontally in a room without wind or external radiations [18]. A terminal aluminum plate was bonded to the conductor and

TABLE 1. Parameters of conductor and enclosure.

Parameter	Conductor	Enclosure
outer diameter/(mm)	180	490
Thickness/(mm)	20	10
Material type	Al alloy A5005-0	Al alloy A6063-T5
Relative permeability	1	1
Reference resistivity/(Ω·m)	2.9×10^{-8}	3.32×10^{-2}
Temperature coefficient of Resistivity/(1/℃)	0.004	0.004
Thermal conductivity/ [W/(m·℃)]	205	209
Specific heat capacity/ [J/(kg·℃)]	900	900
Density/(kg/m^3)	2690	2700
Coefficient of thermal expansion	2.3×10^{-5}	2.3×10^{-5}

TABLE 2. Gas parameters.

Parameter	SF_6	Air
Relative permittivity	1	1
Relative permeability	1	1
Conductivity/(S/m)	0	0
Thermal conductivity/ [W/(m·℃)]	1.206×10^{-2}	2.44×10^{-2}
Specific heat capacity/ [J/(kg·℃)]	665	1 005
Dynamic viscosity/(Pa·s)	1.42×10^{-5}	1.72×10^{-5}

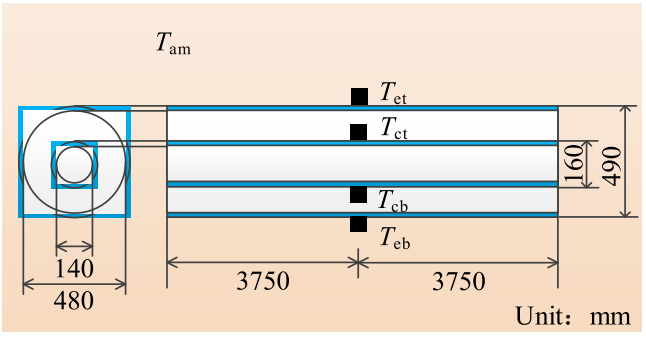

FIGURE 4. Temperature rise experiment of 500 kV GIL.

enclosure so that the conductor current would return through the enclosure. In the experiment, a high alternative current, generated by current transformers, was applied to the GIL conductor with a very low voltage till it reached a steady state [18]. And then, as shown in Fig. 4, the temperature at the top and bottom of enclosure (T_{et} and T_{eb}), the temperature at the top and bottom of conductor (T_{ct} and T_{cb}), and the ambient temperature T_{am} were measured with temperature thermocouple. Here, GIL element is applied with different currents and under different gas pressure conditions, while experimental data of four operation restrictions (I∼IV) are given in Table 3.

TABLE 3. Temperature measurement data of GIL element.

Experimental restriction	I	II	III	IV
Gas pressure/MPa	0.05	0.35	0.35	0.35
Load current/A	5300	2600	4400	5600
Ambient temperature/℃	23	26	16	24
T_{ct}/℃	89	41	57	84
T_{cb}/℃	89	41	57	84
T_{et}/℃	52	34	37	56
T_{eb}/℃	45	31	32	46

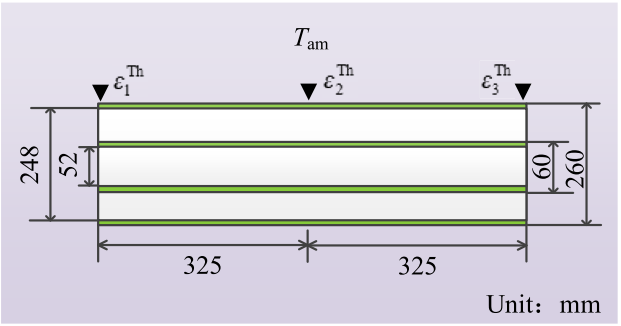

FIGURE 5. Thermal strain experiment.

The thermal strain experiment was carried out in a room without wind or external radiations [12] as shown in Fig. 5. The experimental system was mainly composed of GIL, a high-current generator (HYDDN-200/10000 A with 200 kVA rated capacity and 10 kA rated output current), a static strain demodulator (YSV8316) and resistance strain sensors. A high alternative current was applied to the GIL conductor with a very low voltage till it reached a steady state, and then the axial thermal strain, which means the axial thermal expansion displacement relative to the 1 m element length, is measured at GIL enclosure with the resistance strain sensors. And the experimental data of four experimental restrictions (I∼IV) are given in Table 4.

TABLE 4. Temperature measurement data of GIL element.

Experimental restriction	I	II	III	IV
Gas pressure/MPa	0.5	0.5	0.5	0.5
Load current/A	1000	1500	2000	2400
Ambient temperature/℃	24.8	25.1	25.4	25.9
ε_1^{Th}	74.3	155.8	285.9	377.9
ε_2^{Th}	75.4	156.9	286.8	380.0
ε_3^{Th}	74.1	155.6	285.6	377.6

B. SIMULATION FLOW OF MULTI-PHYSICAL FIELD

According to the mathematical model in section II and the geometric model in section III, multi-physical fields of 500 kV GIL is simulated by COMSOL Multiphysics in desktop workstation with Inter Xeon W-2145 CPU (3.7 GHz) and 64 G RAM.

The laminar flow model is chosen to solve fluid field because Grashov number Gr is calculated as $4.52^{*}10^{6}$, which is less than the threshold $5.76^{*}10^{8}$ (a value lower than this will use laminar model while a value higher than 4.65×10^{9} will use turbulence model) [19] for natural convection.

The calculation process is illustrated in Fig. 5. Here, as a dependent variable, the electric potential is solved separately. However magnetic-thermal-fluid field is directly coupled while the thermal-stress field is sequentially coupled, the solution of the equations is more complex.

In order to ensure convergence of magnetic-thermal-fluid filed, the separation and iterative methods are used. Specifically, the equations of magnetic field are solved and current loss is calculated in frequency domain while the steady state equations of thermal-fluid field are solved based on the current loss. The calculated temperature is used to correct the metal conductivity and current loss, and the magnetic equations and thermal-fluid equations are solved by iteration. Finally, for thermal field and stress field is sequentially coupled, thermal expansion displacement is solved via the temperature simulated. By using the frequency-domain to steady-state solver in COMSOL, one can realize the convergence of the equations.

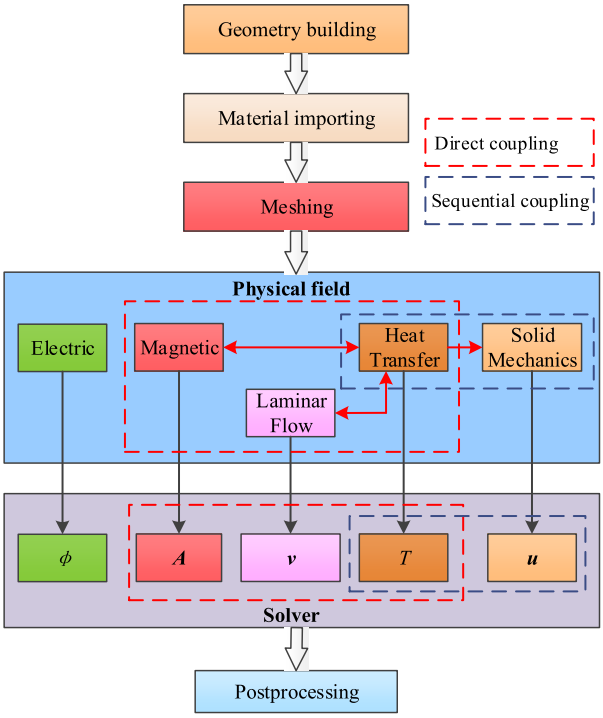

FIGURE 6. Simulation process chat.

C. SIMULATION RESULTS OF ELECTRIC AND MAGNETIC FIELDS

When phase voltage is 289 kV, conductor current is 5600 A and SF_6 gas pressure is constant 0.35 MPa (the following analysis for 500 kV GIL follows this condition unless otherwise specified), distribution of electric field and magnetic

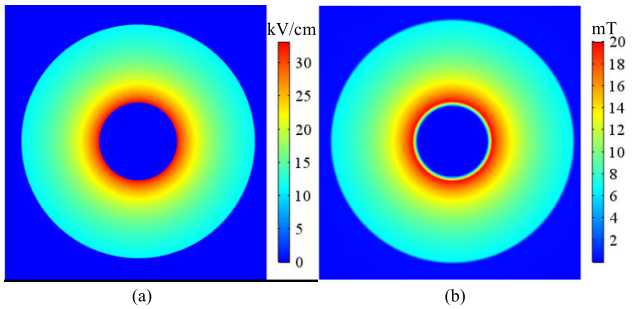

FIGURE 7. Simulation results of electric and magnetic fields. (a) Electric intensity distribution; (b) Magnetic flux density distribution.

field is demonstrated in Fig. 7 while current density of conductor and enclosure are given in Fig. 8.

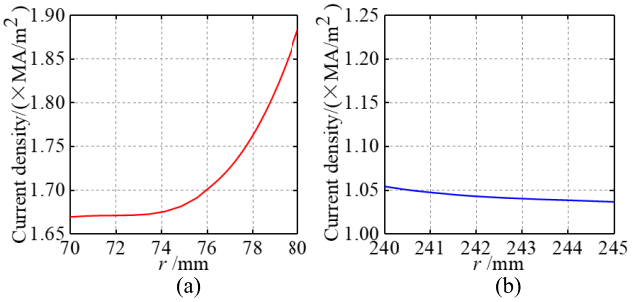

FIGURE 8. Current density distribution of conductor and enclosure of GIL. (a) Conductor; (b) Enclosure.

As shown in Fig. 7, due to shielding effect of enclosure, electric field intensity and magnetic flux density outside GIL are very low, so electromagnetic effect between each phase and each loop of GIL is weak, and electromagnetic field outside enclosure can be ignored.

As shown in Fig. 8, r is the distance to the center of GIL. In terms of distribution of current density, from the perspective of radial section, conductor current is concentrated in its outer ring, while enclosure current is in its inner ring. However, their integral values over the cross-section are very close. The difference of current density in different positions of conductor is higher than that of enclosure, namely, skin effect of current density in conductor is more significant. The reason is that conductor thickness is 10 mm, while enclosure thickness is 5 mm, and skin depth of aluminum is approximately 11.74 mm (50Hz) [20], so skin effect of conductor is more significant.

D. SIMULATION RESULTS AND EXPERIMENTAL VERIFICATION OF THERMAL FIELD

1) CORRECTNESS OF MAGNETIC-THERMAL-FLUID SIMULATION BASED ON EXPERIMENTS

Based on the simulation of GIL element with different air pressure and load current, a comparison between temperature experimented and simulated is presented in Fig. 9.

It can be seen that the calculated temperature is basically consistent with the experimented one, which validates the correctness of thermal field simulation. Considering the

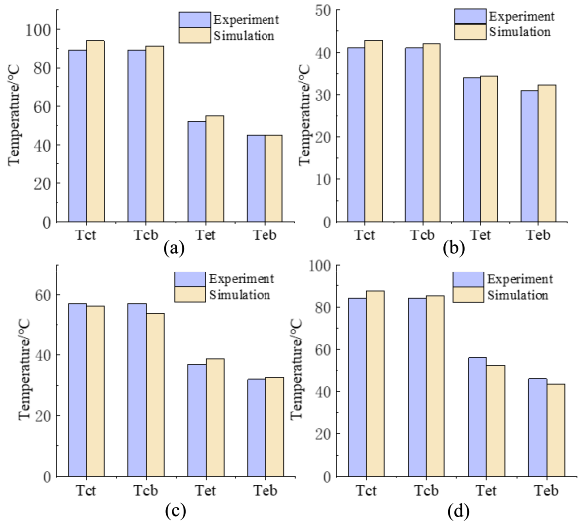

FIGURE 9. Experimental and simulated values of GIL temperature. (a) restriction I; (b) restriction II; (c) restriction III; (d) restriction IV.

thermal field is directly coupled with magnetic and fluid field, the correctness of the magnetic-thermal-fluid field simulation is verified as well.

2) SIMULATION AND ANALYSIS OF THERMAL FIELD

When gas pressure is 0.35 MPa, load current is 5600 A and ambient temperature is 24 °C (Restriction IV), temperature distribution is given in Fig. 10. In addition, the calculated temperature distribution inside GIL at different core angles and distances is shown in Fig. 11.

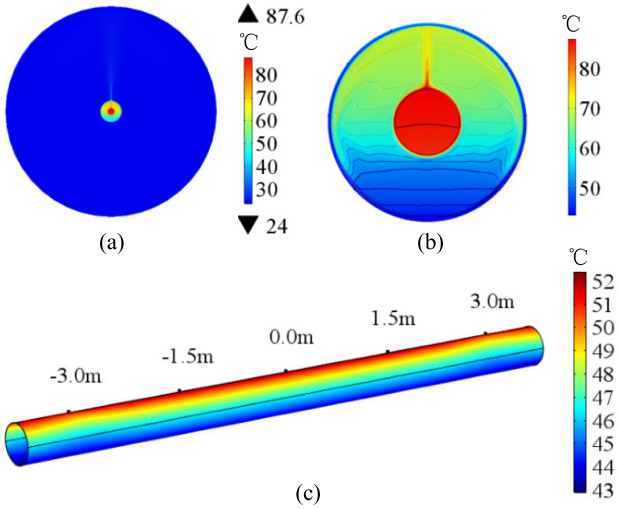

FIGURE 10. Thermal field simulation results of GIL. (a) Temperature distribution in simulation domain; (b) Internal temperature distribution; (c) Enclosure temperature distribution.

As shown in Fig. 10(a), for the outside air of GIL, temperature near the top of enclosure is the highest. In vertical direction, air temperature distribution is inverted "fishtail" and slowly decreases outward, while air temperature in other directions is basically ambient the same as the temperature.

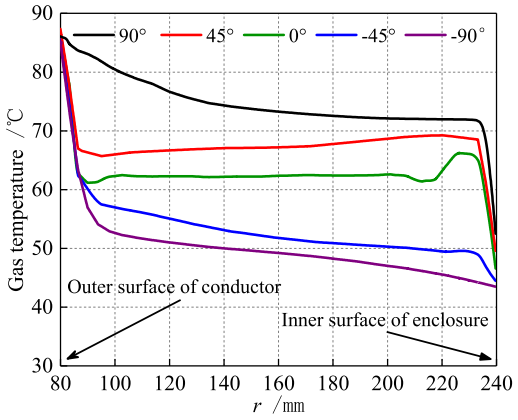

FIGURE 11. Gas temperature of Internal GIL at different core angles and distances.

For SF_6 gas temperature in GIL, it can be seen from Fig. 10(b) that its temperature distribution is bilaterally symmetrical, and temperature in the upper half is higher than that in the lower half.

From axial temperature distribution shown in Fig. 10(c), it can be seen that temperature at top of enclosure is generally higher than that at the bottom, and temperature distribution along axial direction is basically uniform with a slight change near basin insulators (± 3.0 m).

It can be seen from Fig. 11 that gas temperature changes rapidly when it is close to outer surface of conductor and inner surface of enclosure, that is when $r \in$[80 mm, 100 mm]∪[230 mm, 240 mm], temperature decreases rapidly. In addition, at center angle of 0 °, when $r \in$[220 mm, 240 mm], temperature increases significantly and then decreases rapidly with the increase of r, which is caused by the circular gas flow in this area, shown in Fig. 11(b).

E. SIMULATION RESULTS OF FLUID FIELD

Simulation indicates that gas mainly flows along radial direction, but almost not along axial direction, so only the radial gas flow is illustrated in Fig. 12.

Fig. 12(a) shows that external air rises upward from GIL bottom to the top along its enclosure, then diffuses and flows upward. Its distribution is in the shape of "fishtail", which is consistent with air temperature distribution outside enclosure in Fig. 10(a). Here, computation ability of workstation and calculation amount of model are considered to select computation domain. It can be seen that computation domain is not large enough here, however, this paper focuses on the multi-physical fields in and around GIL which is influenced weakly by inaccurate calculation near domain boundary.

As shown in Fig. 12(b), SF_6 gas rises from the bottom to the top along surface of conductor, then rises to the enclosure, descends to the bottom along the inner surface of enclosure, and finally flows back to conductor bottom.

Comparing fluid field in Fig. 12(b) with heat field in Fig. 10(b), one can observe that their distribution is very similar. In particular, a higher temperature results in a higher gas flow velocity, and vice versa.

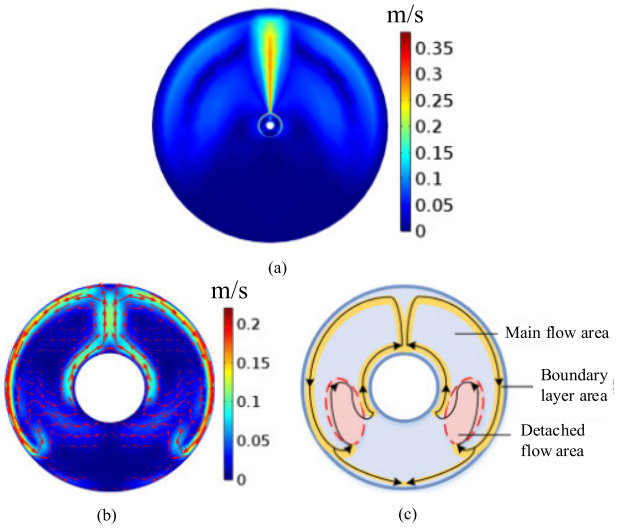

FIGURE 12. Fluid field simulation results of GIL. (a) Flow velocity distribution in simulation domain; (b) Internal flow velocity distribution; (c) Division of fluid flow area.

SF_6 gas flow velocity is relatively high in the area close to boundary and relatively low in other areas. The fluid field can be divided into main flow, boundary layer and detached flow, as demonstrated in Fig. 12(c). Here, gas flow velocity in boundary layer area varies radially, while radial velocity gradient in main flow area is almost 0. Gas begins to disengage from solid surface and flows circularly in detached flow area, which has little influence on the whole flow field, it can still be regarded as laminar flow.

F. SIMULATION RESULTS AND EXPERIMENTAL VERIFICATION OF STRESS FIELD

1) CORRECTNESS OF THERMAL-STRESS SIMULATION BASED ON EXPERIMENTS

Based on the thermal strain experiment, a comparison between thermal strain measured and simulated is presented in Fig. 13. It can be seen that the calculated thermal strain is basically consistent with the measured one, which validates the correctness of thermal-stress field simulation.

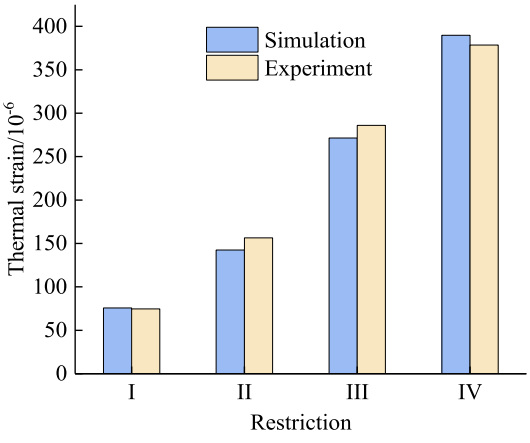

FIGURE 13. Experimental and simulated values of thermal-strain.

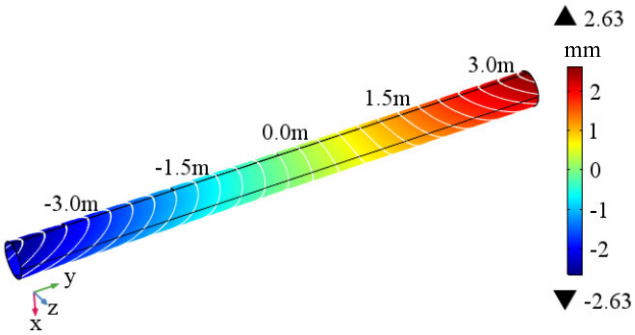

FIGURE 14. Distribution of thermal expansion displacement field of GIL enclosure.

2) SIMULATION AND ANALYSIS OF THERMAL FIELD

To study axial thermal expansion displacement of GIL enclosure, its stress field is simulated with the assumption that the middle of GIL (0.00 m) is fixed, i.e. this point is set as a fixed restraint in axial direction, and the both terminals (+3.75 m and −3.75 m) are considered as linear rigid spring [21]. Simulation results are provided in Fig. 14.

Fig. 14 shows that thermal expansion displacement is larger in upper part and smaller in lower part, which is caused by the uneven temperature distribution of GIL enclosure shown in Fig. 10(c). One can see that when load current is 5600 A, accumulated displacement at top of enclosure terminals reaches +2.63 mm, while that moves +1.96 mm at its bottom, and the average displacement is +2.28 mm. Since enclosure is axial symmetrically, displacement of the other end is equal in size but in opposite direction. For the GIL length is 7.5 m, its average thermal expansion displacement of enclosure under 5600 A load current is about 0.608 mm per meter.

A higher enclosure temperature and a longer length of GIL will lead to a larger total displacement. Because thermal expansion displacement at top and bottom of enclosure is different, asymmetric deformation will occur in the enclosure, the longer GIL length is, the heavier asymmetric deformation is. Therefore, GIL element length should be restricted to reduce the accumulation of thermal expansion displacement while expansion joints should be configured to compensate thermal expansion.

V. ANALYSIS OF RELATED PHYSICAL EFFECTS

A. PROXIMITY EFFECT

GIL temperature rise experiment and the above simulation are designed for a single GIL element without interactions between phases. In fact, GIL runs in at least one loop (three phases). Considering the influence caused by adjacent phases, thermal field and fluid field of three-phase horizontally laying GIL are studied, the results are shown in Fig. 15. Here, gas pressure is 0.35 MPa, phase voltage is 289 kV, current remains 5600 A, and phase sequence is A/B/C from left to right with an interval space of 0.8 m.

As shown in Fig. 15(a), when GIL operates in three-phase horizontal arrangement, temperature distribution just

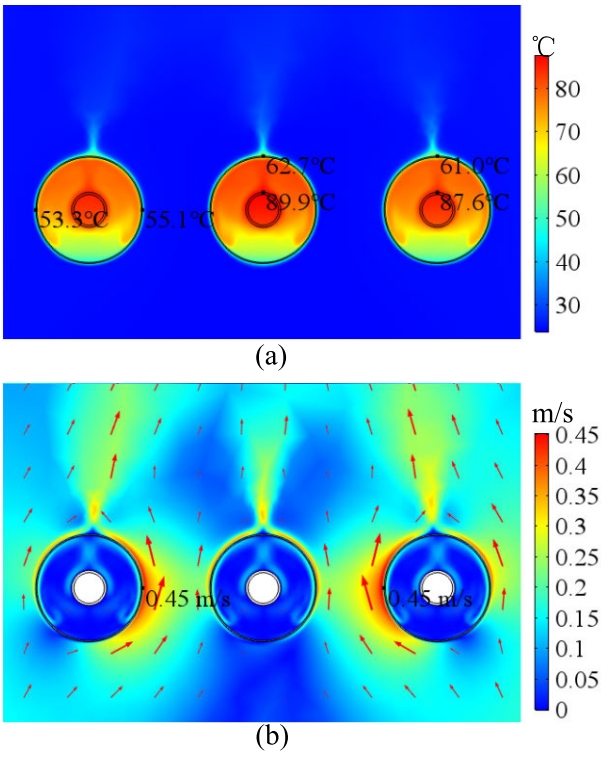

FIGURE 15. Simulation results of three-phase GIL. (a) Temperature; (b) Flow velocity.

changes slightly compared with single-phase operation shown in Fig. 10(b). The temperature of the middle GIL is 3% higher than that of left and right GIL at the same position. Meanwhile, for the left or right GIL, temperature distribution of enclosure is slightly bilaterally asymmetric with about 2 °C temperature difference.

Fig. 15(b) demonstrates that in comparison with single-phase operation, SF_6 flow velocity does not change significantly, while air flow velocity around GIL increases dramatically, especially the GIL interphase air with a 0.45 m/s maximum flow velocity. Air flows upward from enclosure top forming a ''fish tail'', while air above left and right GIL shifts slightly to the middle.

To summarize, the influence of thermal field and fluid field between three-phase GIL results in proximity effect. In normal operation, adjacent phase will affect heat dissipation of the intermediate phase, and then increase external air flow velocity. Under this case (restriction IV), compared to single-phase GIL, gas temperature inside middle GIL is about 3% higher while it is 2% higher for the external air.

B. EDGE EFFECT AND INFLUENCE OF ELEMENT LENGTH

Axial temperature distribution of GIL enclosure is basically uniform with a slight change near basin insulators at both terminals, which results in edge effect. Here, GIL element length is modified for simulation and axial temperature distribution at the top of GIL enclosure is described in Fig. 16.

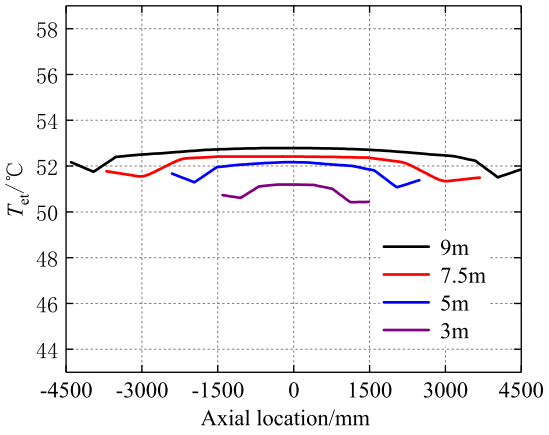

FIGURE 16. Axial temperature distribution at the top of enclosure.

As can be seen from Fig. 16, axial temperature distribution at the top of GIL enclosure is bilaterally symmetrical, generally showing higher temperature in the middle part and lower temperature at both terminals, while temperature decreases at first and then rises near insulators. The reason is that heat accumulation in the middle part of GIL is greater than that in both terminals, and thermal conductivity of basin insulators is larger than that of SF_6 gas.

As GIL element length increases, enclosure temperature increases slightly and edge effect becomes weakened. Note that if one focuses on the middle temperature, that is the highest, the edge effect on middle temperature can be ignored when GIL element length exceeds 7.5 m.

C. COMPRESSION FACTOR

The above simulation considers SF_6 as an ideal gas, neglecting its density deviation, which is reflected by compression factor. When considering compression factor, the gas density under certain pressure and temperature is represented as Eq. (16), which is used in Eq. (14) in section II B.

$$\rho(T) = \frac{PM}{ZRT} \tag{16}$$

where Z is the compression factor and when $Z = 1$, Eq. (16) represents the density of ideal gas.

Gas compression factor under a certain temperature and pressure can be calculated by solving Soave-Redlich-Kwong (SRK) equation via iteration. SRK equation is developed by Soave on the basis of Redlich-Kwong equation, which includes gas eccentric factor and has high calculation accuracy for pure and multi-component mix gas [16].

Under a gas temperature and pressure, iterative SRK equation is written by

$$\begin{cases} Z = \dfrac{1}{1 - bP/ZT} + \dfrac{a(T)}{bRT}\dfrac{1}{1 - ZT/bP} \\ b = 0.08664\dfrac{T_c}{P_c} \\ a(T) = 0.42748\dfrac{R^2T_c}{P_c}[1 + 0.80278(1 - T_r^{0.5})] \end{cases} \tag{17}$$

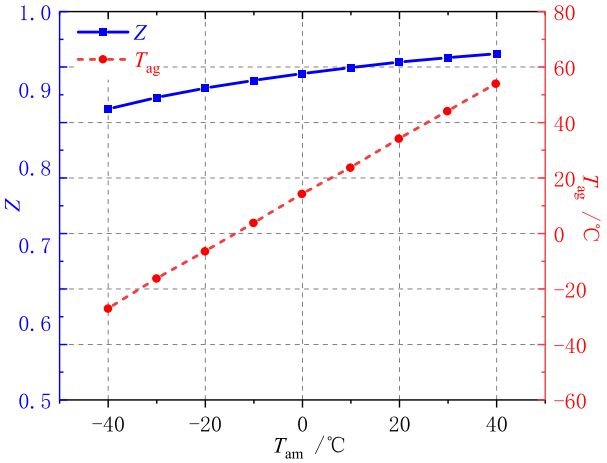

FIGURE 17. SF_6 compression factor and its average temperature at different ambient temperatures.

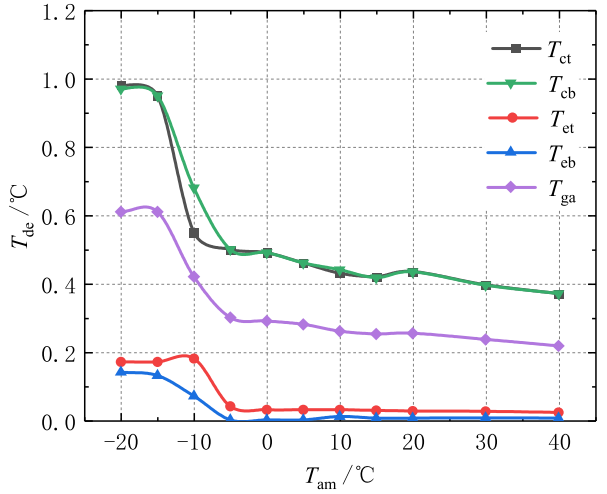

FIGURE 18. Calculating deviation under different ambient temperatures.

where T_c is the critical temperature, P_c is the critical pressure, and T_r is the reduced temperature, respectively.

The iteration process is as follows:

(a) Initial compression factor is assumed as 1;

(b) Average temperature of SF_6 gas is calculated through multi-physical field coupling model;

(c) Compression factor is calculated and updated by Eq. (17), while average temperature of SF_6 gas is calculated by the updated compression factor;

(d) After several iterations, convergence value of average temperature of SF_6 gas and its corresponding compression factor can be obtained.

In this paper, it is simulated under the condition of 289 kV phase voltage, 3000 A current and 0.6 MPa gas pressure. With ambient temperature variation, average temperature of SF_6 gas T_{ag} is provided in Fig. 17, which also shows the change of compression factor Z with ambient temperature.

From Fig. 17, it can be seen that as ambient temperature decreases, both SF_6 gas temperature and compression factor decrease simultaneously. When ambient temperature is much lower, compression factor is less than 1 as shown in Fig. 17.

Therefore, the change of compression factor should be considered in the calculation when ambient temperature is low enough.

In Fig. 18, T_{de} is the deviation of temperature calculated between that with and without considering the change of compression factor.

Fig. 18 shows that under the above operating conditions, when ambient temperature of GIL is above −5 °C, temperature deviations of enclosure, gas and conductor are lower than 0.05 °C, 0.3 °C and 0.5 °C respectively, the influence of compression factor on temperature can be ignored. However, when ambient temperature is lower than −5 °C, temperature deviations are large if compression factor change is ignored, so that compression factor change must be considered.

VI. CONCLUSION

This paper builds a multi-physical field coupling model for 500 kV GIL, electric-magnetic-thermal-fluid-stress coupling simulation is carried out as well. Meanwhile, simulation closely matches experimental results, so that the correctness of simulation model is validated. Moreover, distribution law of each physical field, and proximity effect, edge effect and compression factor of multi-physical coupling field are thoroughly analyzed. The following four conclusions can be drawn.

(a) Conductor current is concentrated in its outer ring while enclosure current is concentrated in its inner ring. Besides, electric intensity and magnetic flux density outside GIL are nearly 0 without proximity effect;

(b) Radial temperature distribution of GIL conductor and enclosure is non-uniform, while temperature at the top is higher than that at the bottom. Meanwhile, axial temperature is basically uniform with a slight change near basin insulators. Proximity effect will cause about a 3% temperature rise in SF_6 gas and a nearly 2% temperature rise in external air. In addition, edge effect will cause temperature decrease at first and then rise slightly near the terminals, as well as weaken edge effect along with the increase of GIL element length. In fact, temperature calculation will be slightly different without considering compression factor. When ambient temperature of GIL is lower than −5 °C, the change of compression factor should not be ignored.

(c) Gas inside GIL flows upward from conductor bottom along with conductor surface, which rises to enclosure through conductor top and descends to enclosure bottom along with inner surface of enclosure, and finally flows back to conductor bottom. Such circulating forms main flow, boundary layer and detachment flow. Meanwhile, proximity effect accelerates the external air and shifts its flow direction.

(d) As GIL temperature distribution is radially non-uniform, distribution of thermal stress field and thermal expansion displacement of enclosure is non-uniform accordingly. Besides, axial deformation of enclosure is asymmetric, which upper part is larger and its lower part is smaller. Lastly, a higher GIL enclosure temperature and a longer length lead to larger thermal expansion displacement.

The GIL multi-physical field is simulated in this paper, and in the future, it can be investigated further about the electromagnetic force, fluid resistance, and the influence of multi-physical field on movement characteristics of free particles, etc.

REFERENCES

[1] Q. R. Ruan and X. P. Xie, *Engineering Design Research and Practice of Gas Insulated Metal Closed Transmission Line*. Beijing, China: Water Resources and Hydropower Press, 2011, pp. 3–4.
[2] T. J. Hammons, V. F. Lescale, K. Uecker, M. Haeusler, D. Retzmann, K. Staschus, and S. Lepy, "State of the art in ultrahigh-voltage transmission," *Proc. IEEE*, vol. 100, no. 2, pp. 360–390, Feb. 2012.
[3] P. Cheetham, A. Al-Taie, S. Telikapalli, T. Stamm, C. H. Kim, L. Graber, and S. Pamidi, "Development of a high-temperature superconducting gas-insulated power cable," *IEEE Trans. Appl. Supercond.*, vol. 30, no. 6, pp. 1–7, Sep. 2020.
[4] T. Magier, M. Tenzer, and H. Koch, "Direct current gas-insulated transmission lines," *IEEE Trans. Power Del.*, vol. 33, no. 1, pp. 440–446, Feb. 2018.
[5] L. C. Li, H. Rao, X. Z. Dong, J. W. Cheng, X. G. Zhao, and B. Luo, "Thoughts and prospects of computational high voltage engineering," *High Voltage Technol.*, vol. 44, no. 11, pp. 3441–3453, 2018.
[6] Y. Qiao, R. Liang, P. Gao, S. Zhu, C. Chen, Y. X. Qin, and X. Tang, "Heat transfer analysis of different conditions for SF_6/N_2 gas-insulated transmission lines," *IEEE Trans. Power Del.*, vol. 5, no. 2, pp. 160–165, Feb. 2020.
[7] D. I. Doukas, T. A. Papadopoulos, A. I. Chrysochos, D. P. Labridis, and G. K. Papagiannis, "Multiphysics modeling for transient analysis of gas-insulated lines," *IEEE Trans. Power Del.*, vol. 33, no. 6, pp. 2786–2793, Dec. 2018.
[8] L. Wang, X. Li, J. Lin, and S. Jia, "Studies of modeling and simulation method of temperature rise in medium-voltage switchgear and its optimum design," *IEEE Trans. Compon., Packag., Manuf. Technol.*, vol. 8, no. 3, pp. 439–446, Mar. 2018.
[9] M. T. Dhotre, J. Korbel, X. Ye, J. Ostrowski, S. Kotilainen, and M. Kriegel, "CFD simulation of temperature rise in high-voltage circuit breakers," *IEEE Trans. Power Del.*, vol. 32, no. 6, pp. 2530–2536, Dec. 2017.
[10] X. W. Wu, N. Q. Shu, H. T. Li, and L. Li, "Contact temperature prediction in three-phase gas-insulated bus bars with the finite-element method," *IEEE Trans. Magn.*, vol. 50, no. 2, pp. 277–280, Feb. 2014.
[11] L. J. Zhong, "Simulation and experimental study of gas insulated metal enclosed transmission lines," M.S. thesis, Dept. Elect. Eng., Suzhou Univ., Suzhou, China, 2016.
[12] J. Wang, C. Chen, Q. M. Li, S. H. Liu, and Z. Y. Wang, "Thermo-mechanical coupling analysis of GIL and its influencing factors," *High Voltage Technol.*, vol. 43, no. 2, pp. 429–437, Jan. 2017.
[13] L.-Y. Chun, F.-F. Meng, Z.-G. Wang, Z.-K. Li, and Y.-M. Li, "Proximity effect and optimized arrangement of cable bundles," *Adv. Technol. Electr. Eng. Energy*, vol. 38, no. 2, pp. 39–41, Jan. 2006.
[14] W. Wu, Y. Xu, X. Xiao, and H. Hu, "Research on proximity effect in measuring error of active electronic voltage transformers," *IEEE Trans. Instrum. Meas.*, vol. 65, no. 1, pp. 78–87, Jan. 2016.
[15] S.-S. Li, Z.-H. Zhang, W. Zhao, S.-L. Huang, and Z. Fu, "Analytical model of electrostatic force generated by edge effect of a Kelvin capacitor based on conformal transformation," *Acta Phys. Sinica*, vol. 64, no. 6, pp. 78–87, 2014.
[16] J. Y. Zhong, X. M. Zhao, B. Z. Li, S. Lin, and Z. X. Geng, "Physical properties calculation of SF_6/CF_4 gas mixture based on SRK equation of state," *High Voltage Elect. Appl.*, vol. 52, no. 12, pp. 48–53, Dec. 2016.
[17] P. Cheng, "Electromagnetic-thermal-mechanical characteristics and characterization method of cable joints with internal defects," M.S. thesis, Dept. Elect. Eng., Chongqing Univ., Chongqing, China, 2016.
[18] D. Minaguchi, M. Ginno, K. Itaka, H. Furukawa, K. Ninomiya, and T. Hayashi, "Heat transfer characteristics of gas-insulated transmission lines," *IEEE Trans. Power Del.*, vol. PWRD-1, no. 1, pp. 1–9, Jan. 1986.
[19] R. W. Breault, "Mass and heat transfer modeling," in *Computational Gas-Solids Flows and Reacting Systems*. Hershey, PA, USA: IGI Global, 2011, pp. 178–202.
[20] L. P. Xu and W. Cao, *Electromagnetic Field and Electromagnetic Wave Theory*. Beijing, China: Science Press, Jul. 2010, pp. 24–25.
[21] J. Snajdr, J. P. Bentley, R. Hauck, and P. Novak, "Stress on outer cable connection of MV gas-insulated switchgear due to cable thermal expansion at rated current," *CIRED-Open Access Proc. J.*, vol. 2017, no. 1, pp. 450–453, Oct. 2017.